# State Selective Enhanced Production of Excited Fragments and Ionic Fragments of Gaseous $Si(CH_3)_2Cl_2$ and Solid-State Analogs following Core-Level Excitation

J. M. Chen,* K. T. Lu,* J. M. Lee, C. I. Ma, and Y. Y. Lee

*National Synchrotron Radiation Research Center, Hsinchu 3007, Taiwan, Republic of China*

(Received 17 September 2003; published 15 June 2004)

State-selective fragmentation dynamics for excited fragments and ionic fragments of gaseous and condensed $Si(CH_3)_2Cl_2$ following Cl $2p$ and Si $2p$ core-level excitations have been characterized. The Cl $2p \rightarrow 15a_1^*$ excitation of $Si(CH_3)_2Cl_2$ induces significant enhancement of the $Cl^+$ desorption yield in the condensed phase and the $Si(CH_3)_2^+$ and $SiCH_3^+$ yields in the gaseous phase. The core-to-Rydberg excitations at both Si $2p$ and Cl $2p$ edges lead to enhanced production of the excited fragments. These complementary results provide deeper insight into the origin of state-selective fragmentation of molecules via core-level excitation.

DOI: 10.1103/PhysRevLett.92.243002 PACS numbers: 32.80.Hd, 33.80.–b, 41.60.Ap, 78.70.Dm

X-ray induced molecular photolysis on surfaces has recently received particular attention because the understanding of this chemistry is essential for the development of evolving technology in the fabrication of microelectronic devices into the nanometer range. With synchrotron radiation of tunable energy, one can prepare the molecule in a well-defined core-excited state and investigate the associated electronic relaxation channels and fragmentation pathways. An intriguing subject in the photochemistry of surfaces is selective photoexcitation and subsequent cleavage of a specific chemical bond in an adsorbed molecule by tuning the photon energy to a particular absorption resonance. The site-specific fragmentation via core-level excitation was identified in several systems [1–5], but not observed in some molecules, such as $Fe(CO)_2(NO)_2$ [6]. The complex relaxation processes for site-selective fragmentation of core-excited molecules are not fully understood and remain the subject of extensive research [7,8]. The fragmented ions discussed in previous reports were predominantly positive ions. The investigation of excited ionic and neutral fragments produced by inner-shell photoexcitation of molecules is still in its infancy [9–11]. At the solid surface, the dissociation dynamics of core-excited molecules might be strongly modified as compared with the gaseous-phase due to electronic interaction with a substrate and/or neighboring molecules [12,13]. Accordingly, to obtain profound insight into the complex relaxation processes of molecular adsorbates on surfaces following inner-shell photoexcitation, coordinated studies of gaseous-phase molecules and solid-state analogues using various experimental techniques are indispensable.

In the present study, by combining the photon-induced dissociation, resonant photoemission, x-ray absorption, ion kinetic-energy distribution, and dispersed fluorescence measurements, the state-selective fragmentation pathways for gaseous and condensed $Si(CH_3)_2Cl_2$ following the Cl $2p$ and Si $2p$ core-level excitations to various resonances have been investigated. The most striking observation is that the Cl $2p \rightarrow 15a_1^*$ excitation of $Si(CH_3)_2Cl_2$ induces significant enhancement of the $Cl^+$ desorption yield in the condensed phase and the $Si(CH_3)_2^+$ and $SiCH_3^+$ yields in the gaseous phase. The core-to-Rydberg excitations at both Si $2p$ and Cl $2p$ edges lead to enhanced production of the excited fragments. These complementary results are crucial for understanding the origin of state-specific fragmentation of molecules following core-level excitation.

The experimental measurements were carried out at the high-energy spherical grating monochromator beam line and the U5 undulator beam line of the National Synchrotron Radiation Research Center (NSRRC) in Taiwan. The experimental details for solid-state related measurements are described elsewhere [14,15]. Highly pure $Si(CH_3)_2Cl_2$ (Merck) was degassed by several freeze-pump-thaw cycles before use. The solid-state photoabsorption spectra were recorded in a total-electron yield (TEY) mode. The ion kinetic energy (not calibrated) was measured by a quadrupole mass spectrometer with a 45° sector field analyzer (Hiden, EQS).

For measurements of gaseous-phase photodissociation and dispersed fluorescence, an effusive molecular beam produced by expanding the gas through an orifice (100 $\mu$m) into the experimental chamber was used. Fragmented ion yields were mass selected through a quadrupole mass spectrometer (Hiden, IDP). Fluorescence was detected with a 0.39-m spectrometer using a $f/1.5$ fused silica extraction optic located normal to and in the plane of polarization of the synchrotron radiation. Because signal levels during dispersed fluorescence measurements were small, the spectral resolution of the spectrometer was set to ~10 nm and the pressure in the effusive beam chamber was kept at $\sim 9 \times 10^{-5}$ Torr. For gaseous-phase photoemission experiments, a supersonic molecular beam is generated by bubbling He gas through $Si(CH_3)_2Cl_2$ in a reservoir and directing it through a continuous-beam nozzle with a seed ratio (concentration ratio of sample gas to He carrier gas) ~10%. Photoemission spectra were

  

measured by a hemispherical electron energy analyzer (VG, Clam4), employing a constant pass energy of 20 eV.

Figures 1(a) and 1(b) show fragmented ion yields following Cl $2p$ core-level excitation for condensed and gaseous $Si(CH_3)_2Cl_2$, respectively, with the Cl $L_{23}$-edge x-ray absorption spectrum for comparison. The absorption peaks labeled 1, 1′ and 2, 2′ in Fig. 1 are ascribed to the Cl $2p \rightarrow 15a_1{}^*$ (Si-Cl) antibonding orbital and Cl $2p \rightarrow 10b_1{}^*$ (Si-Cl) antibonding orbital transitions, respectively. Excitations to Rydberg orbitals are responsible for the absorption peaks labeled 3, 3′. The broad band labeled 4 is attributed to the shape resonance [14]. As shown in Fig. 1(a), the photon stimulated ion desorption (PSID) spectra of $H^+$, $CH_3{}^+$, $SiCl^+$, and $Si(CH_3)_2Cl^+$ follow the Cl $L_{23}$-edge TEY photoabsorption curve of solid $Si(CH_3)_2Cl_2$. In contrast, a significant dissimilarity of the $Cl^+$ PSID spectrum and the Cl $L_{23}$-edge TEY spectrum of condensed $Si(CH_3)_2Cl_2$ is observed. The $Cl^+$ desorption yield shows significant enhancement following the Cl $2p \rightarrow 15a_1{}^*$ excitations when compared to the excitations of Cl $2p \rightarrow 10b_1{}^*$ and Cl $2p \rightarrow$ shape resonance. Besides, the Cl $2p \rightarrow 15a_1{}^*$ excitation effects a slightly enhanced production of $SiCH_3{}^+$ and $Si(CH_3)_2{}^+$, as compared to excitations to Rydberg orbitals.

As shown in Fig. 1(b), the photon-energy dependence of various fragmented ion yields, except $Si(CH_3)_2{}^+$, $SiCH_3{}^+$, and $Si^+$, of gaseous $Si(CH_3)_2Cl_2$ resembles the Cl $L_{23}$-edge photoabsorption spectrum. Especially noteworthy is that the Cl $2p \rightarrow 15a_1{}^*$ excitation of gaseous $Si(CH_3)_2Cl_2$ generates significant enhancement of the $Si(CH_3)_2{}^+$ and $SiCH_3{}^+$ yields, but scarcely any enhancement of the $Cl^+$ yield, as opposed to the condensed phase. Comparison of the $Si^+$ yield spectrum and the Cl $L_{23}$-edge absorption spectrum in Fig. 1(b) shows that Rydberg excitation produces enhancement of the $Si^+$ yield. It is clearly demonstrated from Fig. 1 that there are significant differences in the efficiency for producing fragmented ions, even when these transitions arise from the same atomic site. Hence the character of a bound terminating orbital plays a vital role in determining the photodissociation processes. The ion desorption channels for the condensed phase differ notably from the ion dissociation pathways for the gaseous phase. Accordingly, the comparative studies are clearly imperative for elucidating the detailed photofragmentation dynamics of molecular adsorbates on surfaces.

In Figs. 2(a) and 2(b), the photoemission spectra of condensed and gaseous $Si(CH_3)_2Cl_2$ excited with various photon energies in the vicinity of Cl $2p$ adsorption edge are reproduced. The kinetic-energy scale in Fig. 2 has as reference the vacuum level. The photoemission peaks labeled $A$, $A'$, $B$, and $B'$ are attributed to spectator Auger peaks, whereas feature $D$ corresponds to the normal Auger peak. The most striking feature in Fig. 2 is the pronounced intensity of the spectator Auger peaks

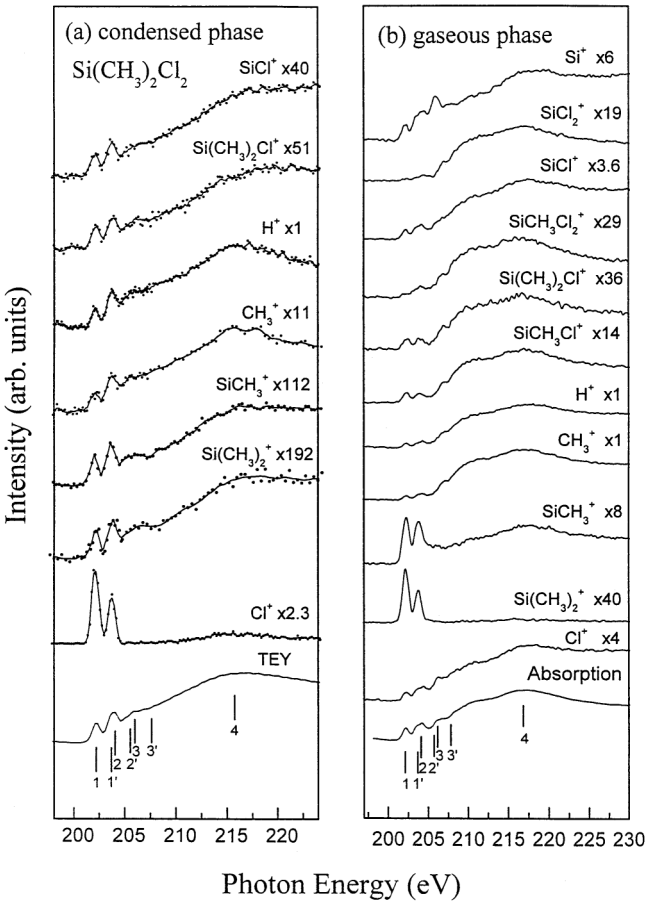


FIG. 1. (a) PSID spectra of condensed $Si(CH_3)_2Cl_2$ via Cl $2p$ core-level excitation along with Cl $2p$-edge TEY spectrum. (b) Photon-energy dependence of various fragmented ion yields of gaseous $Si(CH_3)_2Cl_2$ at the Cl $2p$ edge together with photoabsorption spectrum.

labeled $A$, $A'$, $B$, and $B'$, when the photon energies vary through the core-to-valence resonances. This result reveals that the spectator Auger transitions are the dominant decay processes following core-to-valence excitation, which produce dominantly two-hole, one-electron ($2h1e$) states. In contrast, the shape-resonance excitation was followed by the normal Auger decay. In addition, for Rydberg excitations, feature $C$ in Fig. 2(b) exhibits the same kinetic energy as the normal Auger peak. As noted from Fig. 2, the spectator Auger peaks via core-to-valence excitation have two components. The spectator Auger peaks marked $A$, $A'$ and $B$, $B'$ correspond to the spectator Auger transitions following the Cl $2p \rightarrow 15a_1{}^*$ and Cl $2p \rightarrow 10b_1{}^*$ excitations, respectively. This implies that the spectator electron is localized at the respective valence orbital during the Auger decay. Accordingly, a close resemblance of the photon-energy dependence of various fragmented ion yields and the Cl $L_{23}$-edge absorption spectrum of gaseous and condensed $Si(CH_3)_2Cl_2$, as shown in Fig. 1, is attributed to the Auger decay of core-excited states and the subsequent Coulomb repulsion of multi-valence-hole final states.

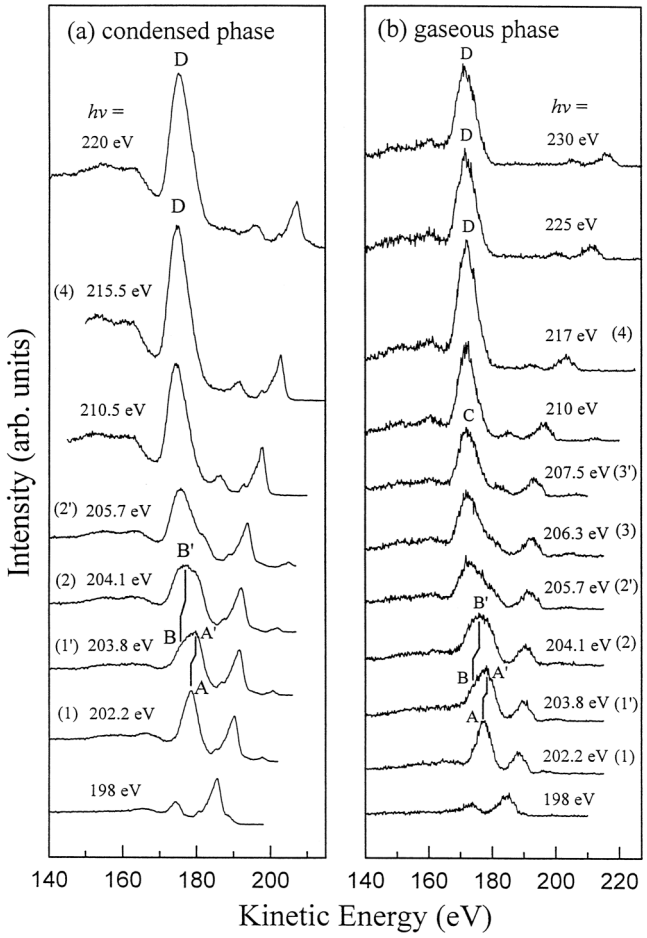


FIG. 2. Auger decay spectra of (a) condensed and (b) gaseous $Si(CH_3)_2Cl_2$ excited with various photon energies near the Cl $2p$ edge. The photon energy used for excitation is indicated in each spectrum. The number indicated in each spectrum corresponds to an absorption peak marked in the absorption spectrum in Fig. 1.

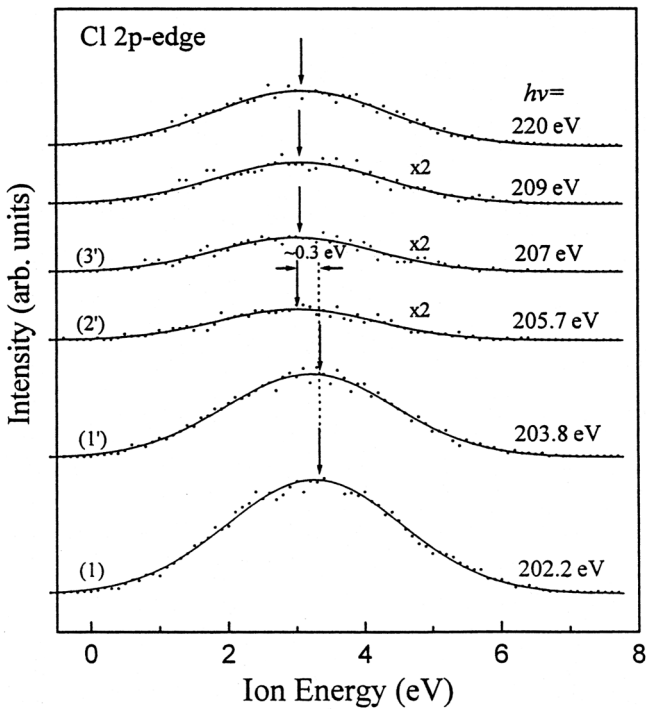


FIG. 3. $Cl^+$ kinetic-energy distributions of condensed $Si(CH_3)_2Cl_2$ following Cl $2p$ core-level excitation. The photon energy used for excitation is indicated in each spectrum. The number indicated in each spectrum corresponds to an absorption peak marked in the TEY spectrum in Fig. 1(a).

The ion kinetic-energy distribution for an adsorbate on a surface via core-level excitation is related to the steepness of the potential energy curves of the precursor core-excited states or the electronically relaxed states [16]. In Fig. 3, the $Cl^+$ kinetic-energy distributions of condensed $Si(CH_3)_2Cl_2$ following Cl $2p$ core-level excitations are reproduced. As noted, the $Cl^+$ ion energy distribution via the excitation Cl $2p \rightarrow 15a_1{}^*$ is shifted to greater energy ($\sim$0.3 eV) compared to that following the excitations Cl $2p \rightarrow 10b_1{}^*$ and Cl $2p \rightarrow$ shape resonance. Because of smaller rates of ion reneutralization, the greater $Cl^+$ kinetic energy at the $Cl(2p)^{-1}15a_1{}^*$ resonance of condensed $Si(CH_3)_2Cl_2$ leads to significant enhancement of $Cl^+$ desorption yield. Because $Si(CH_3)_2{}^+$ and $SiCH_3{}^+$ are more massive than $Cl^+$, the slower departure speed of $Si(CH_3)_2{}^+$ and $SiCH_3{}^+$ from the surface and rapid ion reneutralization greatly diminish the ion yield. Accordingly, unlike the $Cl^+$ spectrum, the Cl $2p \rightarrow 15a_1{}^*$ excitation of condensed $Si(CH_3)_2Cl_2$ leads to only a slight enhancement of the $Si(CH_3)_2{}^+$ and $SiCH_3{}^+$ yields. In the gaseous phase, the ion reneutralization rate is much smaller. As a result, the Cl $2p \rightarrow 15a_1{}^*$ excitation of gaseous $Si(CH_3)_2Cl_2$ induces a substantially enhanced production of $Si(CH_3)_2{}^+$ and $SiCH_3{}^+$, and presumably neutral Cl radicals. Besides, excitations of Si $2p$ to the $15a_1{}^*$ state of gaseous $Si(CH_3)_2Cl_2$ also produce significant enhancement of $Si(CH_3)_2{}^+$ and $SiCH_3{}^+$ yields [17]. Accordingly, after spectator Auger decay of resonant Si $2p$ and Cl $2p$ core-excited states of gaseous $Si(CH_3)_2Cl_2$, the subsequent electronically relaxed $2h1e$ final states with a spectator electron localized in a strong antibonding orbital lead to significant enhancement of specific ion fragments. A similar phenomenon was found for $Si(CH_3)_{4-n}Cl_1$ ($n = 1, 3$), $SiHCH_3Cl_2$ (Si $2p$ and Cl $2p$ edges), etc. [17].

In Fig. 4(a), the dispersed fluorescence spectrum of gaseous $Si(CH_3)_2Cl_2$ obtained from excitation with 230-eV photons is displayed. The sharp peaks between 200 and 300 nm are due to emission from excited Si atoms [18]. The emission peak at 431 nm is identified as the CH(A-X) (0,0) band [19]. The 656-nm peak corresponds to the $H(n = 3) \rightarrow H(n = 2)$ transition. The 390-nm peak is ascribed to overlapping emission of excited $Si^+$ and CH fragments [18,19]. Some emission features are due to a second-order light contribution, as indicated in Fig. 4(a). Figures 4(b) and 4(c) show yields of the most intense

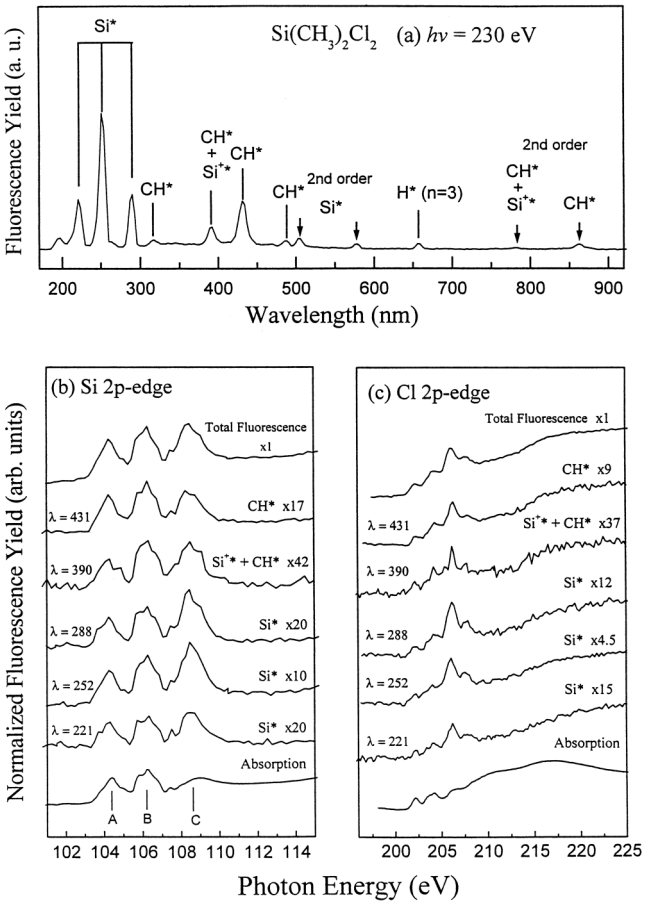


FIG. 4. (a) Dispersed fluorescence spectrum of gaseous $Si(CH_3)_2Cl_2$ following excitation with 230-eV photons. Photon-energy dependence of various excited fluorescing fragments and total fluorescence yield at the (b) Si $2p$ and (c) Cl $2p$ edge with the corresponding photoabsorption spectrum.

excited fluorescing fragments observed in Fig. 4(a) following Si $2p$ and Cl $2p$ core-level excitations, respectively. For comparison, the Si $2p$ and Cl $2p$ edges absorption spectra and total fluorescence yield spectra of gaseous $Si(CH_3)_2Cl_2$ are plotted in Figs. 4(b) and 4(c), respectively. The absorption features labeled *A* and *B* in Fig. 4(b) correspond to excitations of Si $2p$ to Si-Cl and Si-C antibonding states, respectively. The higher-energy peak in feature *C* is due to excitation to Rydberg orbitals.

As noted from Figs. 4(b) and 4(c), the excitation spectra of various excited fluorescing fragments and total fluorescence yield spectra differ significantly from the corresponding photoabsorption spectrum. In contrast to previous reports [9,10], excitations to Rydberg orbitals for both Si $2p$ and Cl $2p$ core levels lead to a noteworthy production of excited atomic fragments, neutral and ionic ($Si^*$, $Si^{+*}$), and excited diatomic fragments ($CH^*$). In particular, the excited neutral atomic fragments $Si^*$ are significantly reinforced. This result indicates that, after spectator Auger decay of resonant core-excited molecules, the subsequent $2h1e$ states with an excited Rydberg electron, as opposed to an excited valence electron, are more likely to dissociate into excited-state fragments. A similar phenomenon was found for $Si(CH_3)_{4-n}Cl_n$ ($n = 1, 3, 4$) (Si $2p$ and Cl $2p$ edges), $CH_{4-n}Cl_n$ ($n = 2$–$4$) (Cl $2p$ edges), etc. [17]. Thus, this finding seems to be of a general nature. It also explains why the Rydberg excitation leads to an enhancement in the $Si^+$ yield given in Fig. 1(b), which is consistent with the enhanced fluorescence yield of $Si^{+*}$.

In conclusion, the complementary results of gaseous and condensed $Si(CH_3)_2Cl_2$ obtained with various detection techniques shed new light on the process of selective bond breaking of molecules via core-level excitation.

We thank the NSRRC staff for their technical support. This research is supported by the NSRRC and the National Science Council of the Republic of China under Grants No. NSC 92-2113-M-213-007 and No. NSC 91-2113-M-213-009.

*Authors to whom all correspondence should be addressed.

[1] W. Eberhardt *et al.*, Phys. Rev. Lett. **50**, 1038 (1983).
[2] R. Romberg *et al.*, Phys. Rev. Lett. **84**, 374 (2000).
[3] Y. Baba *et al.*, J. Chem. Phys. **105**, 8858 (1996).
[4] S. Nagaoka *et al.*, J. Chem. Phys. **107**, 10 751 (1997).
[5] M. C. K. Tinone *et al.*, J. Chem. Phys. **100**, 5988 (1994).
[6] M. Simon *et al.*, in *Synchrotron Radiation and Dynamic Phenomena*, edited by A. Beswick (American Institute of Physics, New York, 1992), p. 323.
[7] Y. Baba, Low Temp. Phys. **29**, 228 (2003), and references therein.
[8] I. Nenner and P. Morin, in *VUV and Soft X-ray Photoionization*, edited by U. Becker and D. A. Shirley (Plenum Press, New York, 1996).
[9] R. A. Rosenberg *et al.*, Phys. Scr. **41**, 475 (1990).
[10] M. Meyer *et al.*, Phys. Rev. Lett. **88**, 223001 (2002).
[11] O. Björneholm *et al.*, Phys. Rev. Lett. **84**, 2826 (2000).
[12] R. Romberg *et al.*, Phys. Rev. Lett. **84**, 374 (2000).
[13] D. Menzel *et al.*, J. Phys. Condens. Matter **13**, 11 249 (2001).
[14] J. M. Chen *et al.*, J. Chem. Phys. **108**, 7849 (1998).
[15] J. M. Chen *et al.*, J. Chem. Phys. **118**, 5087 (2003).
[16] R. Weimar *et al.*, Surf. Sci. **451**, 124 (2000).
[17] J. M. Chen *et al.* (unpublished).
[18] W. L. Wiese *et al.*, *Atomic Transition Probabilities: Vol. II Sodium Through Calcium*, NBS, National Standards Reference Data Series—22 (U.S. GPO, Washington, DC, 1969).
[19] C. Ye *et al.*, J. Chem. Phys. **89**, 2797 (1988).